

Cloud-inclusive Aerial Imagery based on Commercial Flights as Remote Sensing Platform

Dinko Zidic, Jelena Culic Gambiroza, Toni Mastelic, and Mario Cagalj, *Member, IEEE*

Original scientific article

Abstract—Earth observation (EO) significantly increased in the second half of the 20th century and continues to advance rapidly, with remote sensing being a key component for gathering Earth-related information. Nowadays, satellites, manned aircraft, helicopters, UAVs and drones are used to capture aerial imagery in a periodic or schedule-based manner. This paper examines the feasibility of creating a novel remote sensing system by mounting cameras on commercial flights. The study evaluates flight coverage, including spatial and temporal resolutions, and considers the impact of clouds on image usability. We have compared flight coverage with cloud-inclusive flight coverage, which represents reduced flight coverage based on cloud quantity. Results show that entire country of Croatia is covered between 95% and 100% during the day and night. However, when clouds are included in the calculation, it is important to consider different altitudes and periods of the year because their distribution is not the same. In a less cloudy month (August), the highest differences between flight coverage and cloud-inclusive flight coverage for high-altitude flights are 70% for the worst-case scenario and 25% for the best-case scenario. Results show it is feasible to use commercial flights as a new remote sensing system.

Index Terms—remote sensing, aerial imagery, commercial flights, flight coverage, clouds, cloud-inclusive flight coverage.

I. INTRODUCTION

EARTH observation (EO) is a process of collecting information about the Earth using remote sensing technologies, and it shows the capability for creating information related to multiple environmental problems [1]. These environmental problems include tracking, monitoring and understanding changes in the atmosphere, oceans, land surface, and ice sheets over time [2]. Additionally, it is used for monitoring crop status and forecasting crop yield [3], analyzing and monitoring of vegetation [4] or monitoring and optimizing transportation routes and urban planning [5]. The UN 2030 Agenda for Sustainable Development, receives support from EO for 31 of 232 indicators and 71 of 169 targets [2]. Furthermore, remote sensing represents a valuable data source for EO and a wide range of applications [6].

A. Remote Sensing

Remote sensing, a key component of EO, is a process of collecting information about objects on or near the Earth's

surface and atmosphere without direct physical contact [7]. This process involves the capture of data from multiple remote sensing platforms, such as satellites, aircraft, unmanned aerial vehicles (UAVs), and drones [8]. The volume of remote sensing data is increasing due to technological advancements of these platforms, with a significant portion of this data appearing as imagery [2].

To begin with, satellite imagery is captured by high-altitude satellites [9]. However, the high altitude causes a decrease in imagery spatial resolution [10], resulting with lower details. Furthermore, satellites offer a wide field of view, enabling them to cover large areas in a single image, but the cost of creating these images is high [9]. Satellites orbit the Earth at regular period, known as temporal resolution that indicates how long it takes to cover the whole Earth [11].

Next, aerial imagery is captured by manned aircraft and helicopters at lower altitudes, resulting in higher resolution imagery [9]. However, their limited coverage area during each flight and irregular capturing period results with limited ability to cover the entire Earth. Furthermore, this method is expensive due to fuel usage, and the need for a pilot [9].

Last but not least, unmanned aerial imagery is captured using remotely controlled aircraft without onboard human pilot, hence cost of capturing these images is the lowest [12], while the spatial resolution of images is highest [13]. The main drawbacks are small capture area due to a reduced field of view [12] and need for manual operation [13]. All these types of remote sensing imagery have uses, and all of them are obtained in periodic or scheduled-based manner [9] [11].

B. Novel Remote Sensing System

The goal of this paper is to examine the feasibility of creating a novel remote sensing system by mounting cameras on commercial flights. This approach would result with possibility to collect data from locations across the globe in a cost-effective way compared to launching remote satellite, high resolution data by improving spatial and temporal resolution, diverse data sources acquired at different altitudes, angles and time of day. All these improvements should provide more comprehensive and timely information about the Earth. This study covers general flight coverage of Croatia by commercial flights representing an area covered by captured imagery, along with temporal and spatial resolution of captured imagery, and to what extent clouds affect captured imagery in visible spectrum. Flight coverage addresses the geographical reach of remote sensing system, clouds can significantly decrease the

Manuscript received September 18, 2023; revised October 23, 2023. Date of publication November 29, 2023. Date of current version November 29, 2023.

D. Zidic, J. Culic Gambiroza, and T. Mastelic are with Ericsson Nikola Tesla, Split, Croatia (e-mails: {dinko.zidic, jelena.culic.gambiroza, toni.mastelic}@ericsson.com). M. Cagalj is with the University of Split, FESB, Split, Croatia (e-mail: mcagalj@fesb.hr).

Digital Object Identifier (DOI): 10.24138/jcomss-2023-0140

usability of remote sensing imagery, so it is essential to inspect the impact of clouds to check usability of acquired imagery. Clouds can obscure the Earth surface, degrading data quality and reliability, making it impossible to capture clear imagery. Persistent cloud cover is problematic for long-term monitoring, where continuous data is essential for understanding trends.

II. RELATED WORK

The authors in [14] examine the use of commercial flights as an airborne platform for remote sensing. The main concept of their idea is to mount cameras on commercial flights to capture remote sensing imagery. To use commercial flights as an airborne platform for remote sensing, a dataset consisting of aircraft trajectory data for one day is used and land coverage across Europe is estimated. Additionally, the temporal and spatial resolutions of aerial imagery for proposed platform, along with the required storage for all of these images is estimated. Results based on one day aircraft trajectory dataset show that Europe is covered 83.28% with the temporal frequency of one image every half an hour, a ground sampling distance of 0.86 $m/pixels$, and storage requirements of 0.6-4 PB depending on camera choice.

Our study builds upon [14] by employing their methodology and expanding it in several ways. We utilize an increased dataset collected over one year, and more importantly, we also consider to what extent clouds affect the accuracy of the estimated results. To the best of our knowledge, there are no existing similar studies that utilize this approach to inspect the feasibility of this concept. Furthermore, this concept of using commercial flights as an airborne platform for remote sensing is already in progress for implementation by company named SkyFlox [15]. The rest of the related work covers an overview of satellites, aircraft, and UAVs as remote sensing platforms.

A. Satellites

Satellites are used as a platform to capture aerial imagery, namely satellite imagery. Over the years, satellite technology in remote sensing has advanced, and now they can provide a comprehensive view of land, oceans, atmosphere, and climate [16]. Additionally, satellite sensors advanced, allowing capturing higher-resolution imagery, multi-spectral and hyper-spectral data [17][18]. United Nations Office for Outer Space Affairs says that there are 8,261 satellites in Space, over half of which are active [19].

The first artificial satellite Sputnik 1 launched in 1957. spent three months in space [20], while a weather satellite Tiros-1 is launched three years after. Further, first civilian satellite for EO known as Landsat 1, launched in 1972. had spatial resolution of 80m and revisit time of 18 days [21]. Landsat becomes the beginning of the satellite series that provide valuable data for EO. Furthermore, Ikonos 1 was the first commercial remote sensing satellite launched in 1999. with a revisit time of 3 days and spatial resolution of 80m [20]. Landsat 9 launched in 2021. has spatial resolution of 30m, expected lifetime of 5 years, and a temporal resolution of 8 days [21].

A specific type of satellite named the geostationary satellite can provide near real-time remote sensing data, but their high

altitude of about 36,000km decreases the resolution of the imagery [22]. For example, GOES-R satellite, that provide imagery of weather patterns and atmospheric conditions could be used to track severe weather events [23]. Nowadays, there are numerous modern satellites used for EO [16]. For example, Airbus launched satellites for the EO named as Pléiades, OneAtlas, and Spot 6/7 [24]. However, Airbus products are commercial type, and there is a price for using their images.

B. Aircraft

Aircraft precedes the UAVs usage for EO and remote sensing. Its initial usage started during World Wars, but increased at the end of 20th century [25]. This remote sensing platform requires the pilot to drive the vehicle while collecting data. During technological advancements, aircraft are increasingly used for remote sensing because new sensors bring improved data capture capabilities [18]. In this case, spatial resolution is better than satellites, but not as good as UAVs.

Some of the aircraft used for EO is NASA Sofia, a specialized Boeing 747 that can also be used for space investigation [20] [26]. An airplane NASA ER-2 is similar to the U2 airplane used for scientific investigation of the atmosphere, climate, and Earth [27]. It has multiple sensors for capturing high resolution aircraft imagery. Additionally, Cessna 206 is a highly prominent commercial aircraft for capturing aerial imagery [28]. All of these aircraft are bound by a limited time they can remain airborne, affected by fuel capacity and weather conditions, resulting in parameter named flight time.

Aircraft became popular platform for use-cases such as remote sensing, high-altitude imaging, and specialized research missions. They offer the advantage of carrying heavy and advanced remote sensing equipment, covering extensive areas, and accommodating complex sensor configurations.

C. UAV

UAVs gained popularity in the late 20th century. When UAVs first appeared, they faced challenges like flight time and the sensors required for data capturing. However, due to technological improvements and advancements in miniaturized sensors, UAVs have become capable of carrying remote sensing payloads [18]. The primary characteristics of UAVs that have improved through time are speed, maximum range, and flight time which reflects the maximum time that UAV can spend in the air [29]. UAVs can carry various types of sensors including digital cameras, multi-spectral sensors (LiDAR), and many others [29]. With these advancements, it became alternative to satellites and aircraft with benefits of low cost and increased spatial resolution.

Multiple types of UAVs are used for EO including drones, multirotors, and fixed-wing UAVs [30]. Drones flight time vary based on its type, hence military drone MQ-C Gray Eagle achieved the longest flight time of 25 hours and a range of 400km [31]. However, professional drones achieved the longest flight time of 10 hours with a maximum range of 200km, while maximum flight time of recreational drones is 40 minutes with a maximum range of 9km [31].

Furthermore, a few UAV examples are WingtraOne with a spatial resolution of $1\text{-}3\text{cm}$ [32] and world-record-breaking high altitude platform station Zephyr developed by Airbus company [33]. It can fly for months at an altitude of 21km and offer spatial resolution of 18cm . UAVs have recently emerged as an important tool for remote sensing in the field of EO. Technological improvements push the limitations of existing solutions and create new opportunities for obtaining high resolution, multi-sensor data to expand the applications of remote sensing in various fields of study [29].

III. METHODOLOGY

In this section we provide an overview of aerial imagery basic characteristics, along with an introduction to the defined aerial imagery types (Section III-A). Then we present in details datasets used in our analysis; flight dataset (Section III-B) and cloud coverage dataset (Section III-C).

A. Aerial imagery characteristics

The four types of resolution that define the characteristics of aerial imagery are spatial resolution, spectral resolution, temporal resolution, and radiometric resolution [14] (Table I). In this paper, we focus on spatial and temporal resolution, as the flyover frequency and altitude impact these characteristics.

However, except for resolution types, the capture time affects aerial imagery as well [34]. The Sun creates shadows on aerial imagery, depending on time capture time, sometimes more shadows are tolerable, but sometimes not [35]. Regarding this, we define aerial imagery types based on capture time, representing a part of the day when the imagery is captured, namely: daytime, nighttime and twilight, which are referred as *solar-based imagery*. In the sequel we provide a rationale for these types.

1) *Aerial Imagery Capture Time*: Generally speaking, aerial imagery types by capture time could be characterized by hours. However, a year has 365 days and four seasons, thus an hour in a different season does not represent the same part of the day. As a result, using hours as a basis for imagery types is problematic, hence new approach is required.

We argue that the solar altitude angle is a better parameter to differentiate aerial imagery types. The term solar altitude angle (θ) represents the angle between the horizontal plane and the line to the Sun (Figure 1a), and can be calculated for any hour of the year [36]. The calculated values depend on the day of the year, time, and observer's location [36]. Therefore,

possible values are between -90° and 90° , where 0° is the Sun phase known as sunrise/sunset, 90° is the Sun phase when the Sun is at its highest point known as zenith, and -90° is Sun phase known as the nadir [37]. Figure 1b shows the relation between the Sun phases and solar altitude angles.

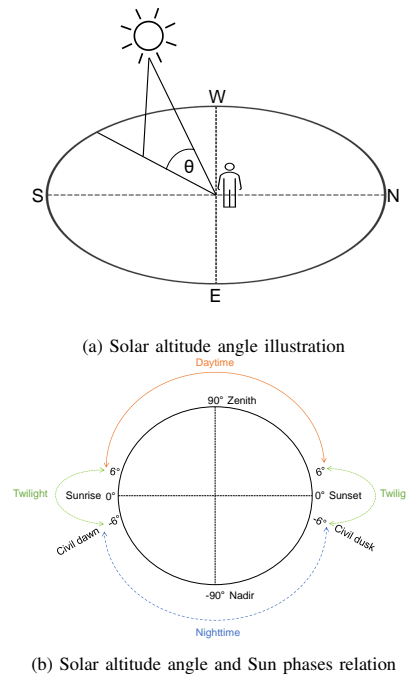


Fig. 1. Solar altitude angle (θ)

Additionally, two Sun phases known as the civil dawn and the civil dusk represent a moment when the center of the Sun is 6° below the horizon in the morning, and a moment when the center of the Sun is 6° degrees below the horizon in the evening, respectively [38]. These two events in one term are named the civil twilight [37].

2) *Solar-based Imagery Types*: Based on findings from the previous section, we have defined three solar-based imagery types that represent a period of the day when they are captured (Figure 1b), namely:

- 1) *Nighttime imagery*: captured during the period between 6° after sunset and 6° before sunrise $[-90^\circ, -6^\circ]$
- 2) *Twilight imagery*: captured during the period between civil dawn and 6° after sunrise, as well as captured during the period between 6° before sunset and civil dusk $[-6^\circ, 6^\circ]$
- 3) *Daytime imagery*: captured during the period between 6° after sunrise and 6° before sunset $[6^\circ, 90^\circ]$

To sum up, nighttime imagery is captured during the night, twilight imagery during dusk and dawn, and daytime imagery during the day. We adjusted the upper bound of twilight (6°) to create a symmetric range of the solar altitude angles that spans a short period after sunset or sunrise, respectively, when shadows are most prominent. Figure 2 depicts distribution of available hours for capturing solar-based imagery types. It can be seen how solar altitude angles are affected by the seasons, resulting in more daytime hours in the summer and spring, and more nighttime hours in winter and autumn. The twilight

TABLE I
AERIAL IMAGERY RESOLUTIONS OVERVIEW

Resolution	Definition
Spatial	minimum object size that can be discern
Temporal	the frequency of capturing new readings
Spectral	the ability of detecting and measuring multiple spectral bands
Radiometric	the ability of identifying small variations in electromagnetic radiation

imagery is characterized by constant duration for almost the entire year since it is the shortest period unaffected by seasons.

B. Flight Dataset

For this paper, we use the commercial Flightradar24 dataset [39], which contains data based on historical aircraft locations. Flightradar24 primarily uses Automatic Dependent Surveillance-Broadcast (ADS-B) receivers to receive flight information broadcasted from aircraft ADS-B transponders. However, the transponder frequency of position updates is different for every part of the flight and it depends on the flight phase (take-off/landing, ascending/descending, cruising), varying from 5 to 60 seconds. Thus, the updating frequency is highly dependent on the altitude and the direction during a flight, because during the cruising phase fewer samples are required to maintain a track of the aircraft position [39].

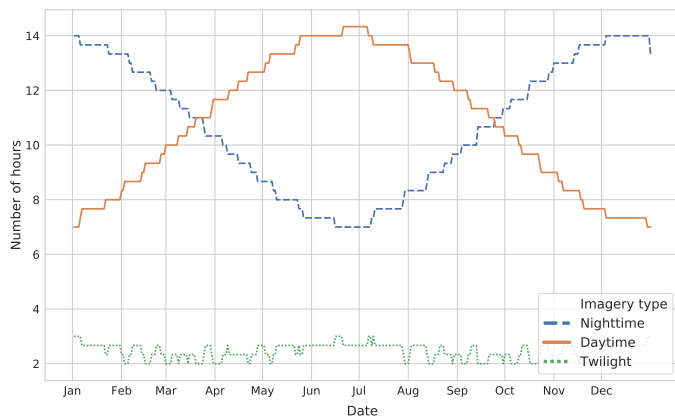


Fig. 2. Solar-based imagery types and hours relation

The Flightradar24 dataset consists of two segments named *trajectory data* and *flight data*. Trajectory data holds the location of the flight based on latitude, longitude, speed, and altitude, usually obtained from an aircraft transponder or calculated if none is available (Table III). The flight data contains metadata information such as aircraft ID, equipment and call sign. The data used in our analysis are collected in a period of one year in the range between 01/01/2019 and 01/01/2020 for flights over Croatia. Overall, the dataset size and calculated dataset statistics can be found in Table IV.

1) *Data Processing*: Before using the dataset for analysis, all non-commercial flights, including private aircraft, non-callsign flights, airport ground vehicles, unidentified flying objects (objects not identified as commercial or private), and grounded flights are removed. Specifically for this, *flight number* and *call sign* are used to identify commercial flights and remove unregistered commercial aircraft. The *flight ID* is used to distinguish different flights and create trajectories for each flight, while *equipment* and *aircraft ID* are used to filter out airport ground vehicles and private aircraft. The steps for data analysis, which include calculating *flight coverage (FC)* as percentage of area covered from a commercial aircraft during flight, data volume, temporal and spatial resolutions of aerial imagery, are as follows:

- 1) The first step is interpolating a dataset containing flight trajectories and polygons. This interpolation is required to obtain field of view of moving camera installed on aircraft (Figure 3). Field of view is used to estimate spatial and temporal resolutions, flight coverage, and number and size of the images captured during the flight (Section III-B2).
- 2) The second step is projecting the land mass and trajectories onto the map to calculate statistics, area size, and flight coverage. In this case, ESPG:3035 (ETRS89) coordinate reference system is used with a Lambert Azimuthal Equal Area (LAEA) [14] map projection.
- 3) The third step is overlapping images to cover an area with multiple images as a common practice in airborne photography to prevent data loss and increase accuracy in image processing (Section III-B3).
- 4) The final step includes dataset clustering to ensure a more fine-grained result. The results of flight coverage, temporal and spatial resolutions, and storage capacity are provided in general as well as in clusters of different altitudes and imagery types.

2) *Interpolating Flight Trajectories*: The goal of this step is to perform interpolation to get field of view (*FOV*) of moving camera. That field of view represents an area that one flight covers (flight trajectories), that is impacted by camera type. Before any calculations, based on the previous analysis [14], camera Imperx T9040 was selected for this research, whose characteristics are shown in Table II.

The first step required to interpolate flight trajectories is to calculate the horizontal and vertical angle of view (AOV_h and AOV_v) for every recorded position in the dataset using Equation 1. The second step is to calculate the horizontal and vertical field of view (FOV_h and FOV_v) for every recorded position in the dataset using AOV calculated values along with altitudes and apply it to Equation 2.

To estimate the flight coverage, spatial and temporal resolutions, FOV_h which represents the horizontal distance in meters, is used to create polygons that represent continuous FOV . Additionally, FOV_v represents the vertical distance in meters and is used to estimate the number and size of the captured images. Figure 3 depicts the interpretation of horizontal and vertical AOV and FOV , as well as their relation with altitude when camera is mounted on an aircraft.

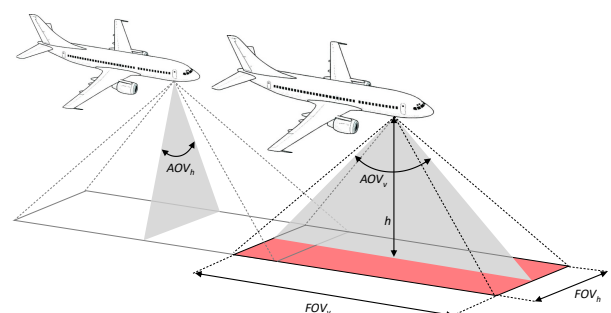


Fig. 3. FOV relation to the (AOV) and altitude h [14]

TABLE II
IMPERX T9040 CAMERA CHARACTERISTICS

Focal length (mm)	CCD width (mm)	CCD height (mm)	Horizontal pixels (#)	Vertical pixels (#)	Image size (MB)	FOV _h (m)	FOV _v (m)
35	47	22	10,440	4,800	207	67.76	34.89

TABLE III
METADATA REFERENCE FOR THE TRAJECTORY DATA SEGMENT

Data field	Description	Example
SnapshotID	Timestamp (Unix time)	1504224761
Altitude	Height above sea level (ft)	40,000
Latitude	Floating point format	45.815
Longitude	Floating point format	15.967
Speed	Ground speed in knots	440

TABLE IV
FLIGHT DATASET STATISTICS

Name	Value
Unique flights	640,911
Unique aircraft	9,410
Total number of points	10,047,093
Average number of points per flight	19
Weighted average speed (km/h)	794.25
Weighted average altitude (km)	9.17

$$AOV[\text{DEGREES}] = 2 \cdot \arctan\left(\frac{s}{2 \cdot f}\right) \cdot \left(\frac{180}{\Pi}\right); \quad (1)$$

where s is width/height of the sensor [mm],
 f is focal length [mm].

$$FOV[\text{METERS}] = 2 \cdot \tan\left(\frac{AOV}{2}\right) \cdot h; \quad (2)$$

where h is altitude [m].

3) *Overlapping the Images*: Aerial imagery is commonly captured with some redundancy by overlapping the images to prevent data loss and increase accuracy in processing. A percentage is used to express an overlap, defined as the amount by which one image covers the area covered by another. There are two types of overlap, called *forward overlap* (O_f) that defines overlap between images along the same line of flight, while *lateral overlap* (O_l) is an overlap between images on adjacent flight lines [14]. Furthermore, suggested forward overlap (O_f) is 60% [40], and it is used to estimate the number of captured images, required to calculate storage capacity.

C. Cloud Coverage Dataset

This section provides information that highlights significance of this study and outlines objective of this paper, i.e. *composite cloud coverage* (CC^*) and *cloud-inclusive flight coverage* (FC^*). In this paper, ERA5 reanalysis is used to get the cloud coverage dataset [41].

The used cloud coverage dataset represents regridded point data in a time interval from 01/01/2019 to 01/01/2020 inside the borders of Croatia. Since the horizontal resolution of ERA5 is $0.25^\circ \times 0.25^\circ$ [41], each point in the grid represent a center

of area sized $25km \times 25km$ for Croatia (Figure 4). Each record in the dataset comprises information for geographic location, time, and *cloud coverage* (CC). Cloud coverage is defined as the percentage of area covered by clouds and ranges from 0 (no clouds) to 1 (full cloudiness). We consider three types of cloud, namely *low* (L), *medium* (M), and *high* (H) (Table V). It is essential to understand that clouds occurrences vary with altitude because humidity, temperature and atmospheric conditions are different at different levels. Additionally, seasonal variations in weather patterns and climate can influence cloud distribution based on different time. In our case there are three ERA5 cloud coverage datasets named *low cloud coverage* (CC_L), *medium cloud coverage* (CC_M), and *high cloud coverage* (CC_H) (Table VI).

TABLE V
CLOUD TYPES BY ALTITUDE RANGES

Type	Notation	Altitude
Low	L	below 2km
Medium	M	between 2km and 6km
High	H	above 6km

TABLE VI
CLOUD COVERAGE DATASET METADATA

Data field	Description	Example
Latitude	Floating point format	43.63
Longitude	Floating point format	15.73
Time	Date-time format of occurred event	2019-01-01 00:00:00
TCC	Cloud coverage	0.5
Type	Indicator for cloud type	L

Finally, we need to estimate a composite cloud coverage to be able to estimate cloud-inclusive flight coverage. Three steps required to achieve that are explained in Section III-C1, III-C2, and III-C3, and they are respectively:

- 1) Transforming the cloud coverage data
- 2) Estimating a composite cloud coverage
- 3) Estimating the cloud-inclusive flight coverage

1) Transforming Point Grid Data to Polygon Grid Data:

As previously stated, cloud coverage data is point grid data with cloud coverage values assigned to each point, where each point in the grid represent a center of area approximately sized $25km \times 25km$. Accordingly, the first step is to transform point grid data to polygon grid data in such a way that one grid point represents the center of the polygon sized $25km \times 25km$. Figure 4 depicts the schema of point grid to polygon grid transformation. Please note that cloud coverage does not reveal the exact location of the cloud within that polygon.

2) *Estimating Composite Cloud Coverage*: After transforming the point grid into polygon grid, the next step is *composite cloud coverage* (CC^*) calculation to estimate cloud-

inclusive flight coverage, as clouds affect flight coverage. For example, a medium cloud coverage of 0 at an altitude of $3km$ does not mean Earth from an altitude of $3km$ is fully visible, because underneath medium clouds there may be low clouds. Clearly, to obtain accurate cloud coverage information all types of clouds must be taken into account. Consequently, *composite low cloud coverage* (CC_L^*) is low cloud coverage, *composite medium cloud coverage* (CC_M^*) combines low and medium cloud coverage, and *composite high cloud coverage* (CC_H^*) combines low, medium, and high cloud coverage.

However, since there is no way to know the exact spatial location of clouds in a polygon, we use three cases to inspect clouds overlapping at different altitudes, as previously explored in [42] [43]. Accordingly, there are three basic idealized assumptions of cloud overlapping named *maximum*, *minimum*, and *random overlap* [42]. The maximum overlap presupposes that different cloud types overlap entirely (Figure 5a), providing best-case scenario, as it assumes full stacking of cloud types. The result of using this assumption is the most optimistic estimation of cloud coverage. The minimum overlap is an assumption where cloud types are observed separately, which means each cloud is considered individually without any overlap (Figure 5b), representing the worst-case scenario. The random overlap is a statistical and probabilistic method that represents a more realistic approach to obtain cloud coverage and assume partial overlap (Figure 5c). It uses the probability of different cloud types overlapping with each other.

We model this problem as follows. First, we assume that occurrences of different cloud types are independent. Then, three different idealized assumptions of clouds overlapping is used to define equations to estimate composite cloud coverage. For maximum overlap assumption it is assumed there is maximum overlap between low, medium, and high clouds, leading to minimal composite cloud coverage (Equation 3). Next, for minimum overlap assumption it is assumed there is no overlap between low, medium, and high clouds, resulting in maximal composite cloud coverage (Equation 4). Finally, for random overlap assumption it is assumed there is overlap estimated by using probabilistic and statistic methods (Equation 5).

- Minimum cloud coverage (if maximum cloud overlap assumption is used)

$$CC^* = CC_{min}^* = \max(CC_L, CC_M, CC_H) \quad (3)$$

- Maximum cloud coverage (if minimum cloud overlap assumption is used)

$$CC^* = CC_{max}^* = \min(1, CC_L + CC_M + CC_H) \quad (4)$$

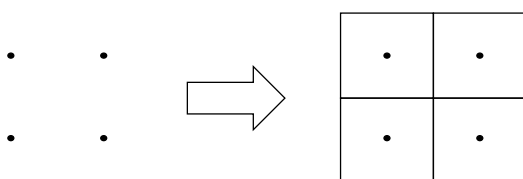


Fig. 4. Point grid to polygon grid - cloud transformation

- Random cloud coverage (if random cloud overlap assumption is used)

$$CC^* = CC_{rand}^* = CC_L + CC_M + CC_H - CC_L \cdot CC_M - CC_L \cdot CC_H - CC_M \cdot CC_H + CC_L \cdot CC_M \cdot CC_H \quad (5)$$

3) *Coalescing Composite Cloud Coverage Data and Flight Coverage*: Finally, if composite cloud coverage is estimated, it can coalesce with flight coverage to obtain a cloud-inclusive flight coverage. Since the cloud coverage is defined for the polygon sized $25km \times 25km$, the cloud-inclusive flight coverage is estimated on a level of the base unit polygon that is exactly $25km \times 25km$. This problem is approached as follows; we assume that clouds and flight occurrences are independent, and based on that we introduce three distinct conceptual assumptions that illustrate the potential overlap between clouds and FOV_h of camera mounted on the aircraft.

The first assumption, denoted as maximum overlap represents the worst-case scenario wherein clouds totally obscure FOV_h , resulting in minimal to no cloud-inclusive flight coverage (Figure 6a). The second assumption, referred to as minimum overlap depicts the best-case scenario where clouds have no or minimal overlap with FOV_h , (Figure 6b). This scenario optimally maximizes cloud-inclusive flight coverage by minimizing any potential cloud interference. Lastly, the random overlap represents the most realistic scenario of partial overlap between clouds and FOV_h by considering probabilistic and statistical methods (Figure 6c). By modeling the problem under these three defined assumptions, we provide analysis that includes all, optimistic, realistic, and pessimistic perspectives on the overlapping between clouds and FOV_h .

As a result, Equations 6, 7 and 8 define how to estimate *cloud-inclusive flight coverage* (FC^*) based on selected flight overlap assumption, for maximum, minimum, and random overlap, respectively. Cloud coverage that goes into the equation is one of the three composite cloud coverage that depends on the flight altitude for which we are calculating cloud-inclusive flight coverage and used cloud overlapping idealized assumption.

- Minimum cloud-inclusive flight coverage (if maximum overlap assumption is used)

$$FC^* = FC_{min}^* = \max(0, FC - CC^*) \quad (6)$$

- Maximum cloud-inclusive flight coverage (if minimum overlap assumption is used)

$$FC^* = FC_{max}^* = \min(FC, 1 - CC^*) \quad (7)$$

- Random cloud-inclusive flight coverage (if random overlap assumption is used)

$$FC^* = FC_{rand}^* = FC - FC \cdot CC^* \quad (8)$$

For example, if the flight coverage inside a polygon sized $25km \times 25km$ is 25%, and the composite cloud coverage calculated using random overlap assumption is 35%, the cloud-inclusive flight coverage using random overlap assumption would be 16.25% (Figure 7). To summarize, this reduces flight coverage based on cloud coverage because the camera cannot see through clouds, which affects flight coverage directly.

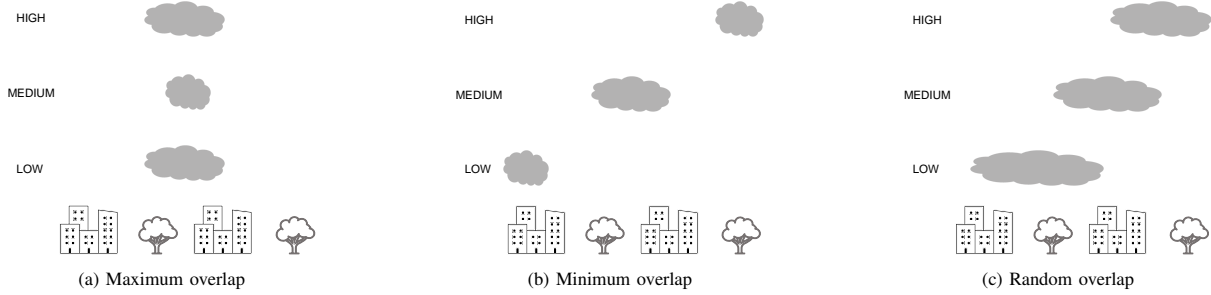


Fig. 5. Clouds overlapping idealized assumptions

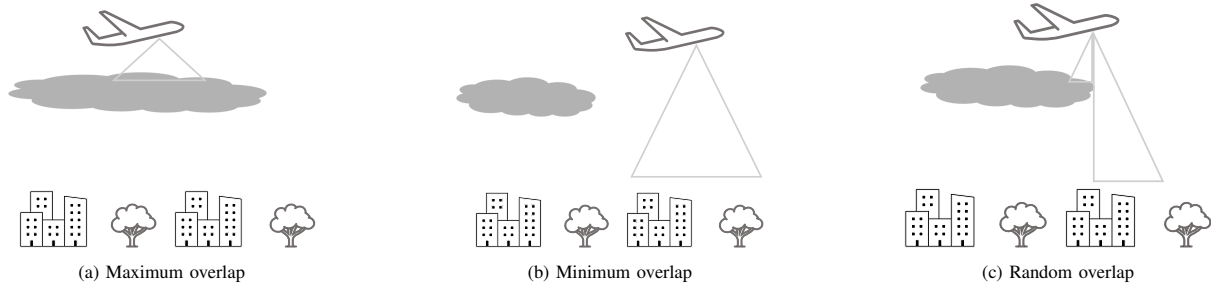


Fig. 6. FOV_h of camera mounted on the aircraft and clouds overlapping idealized assumptions

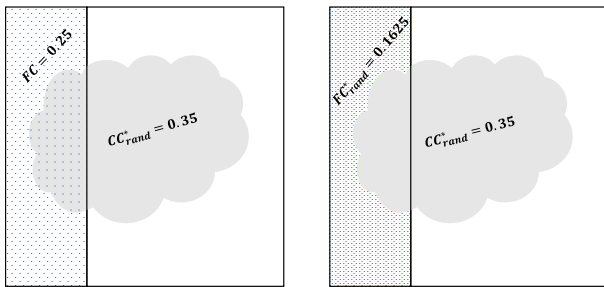


Fig. 7. Cloud-inclusive flight coverage overview

IV. RESULTS

This section presents the results of applying defined methodology (Section III) to the cloud coverage and flight datasets. All results are calculated for entire country of Croatia, assuming Imperx T9040 camera is mounted on commercial flights. The results show overall flight coverage (FC), the impact of capture time and altitude on flight coverage, overall cloud coverage (CC), and its impact on flight coverage. Further, the temporal and spatial resolutions and storage required for all captured imagery, are estimated.

A. Flight Coverage

Flight coverage denotes the area covered by captured aerial imagery. Figure 8a shows all flight polygons over Croatia. The color intensity represents the number of flights that pass over a specific area in a year. It is clear that the entire Croatia is well covered during one year. Figure 8b shows a flyover frequency above Croatia in one year. The majority of flyovers are concentrated between 20,000 and 40,000 appearances. Furthermore, a few flyovers exceeded the majority of flyovers ranging between 60,000 and 80,000 and may be noticed on Figure 8a in northeast and northwest border. Moreover, overall

daily FC is above 98.6% throughout the year, with FC increasing between April and October (Figure 9a).

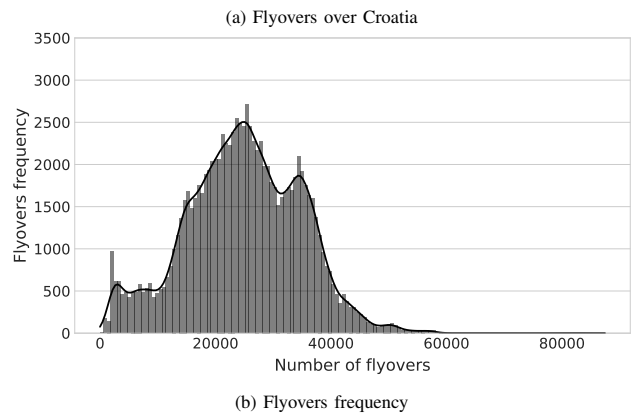
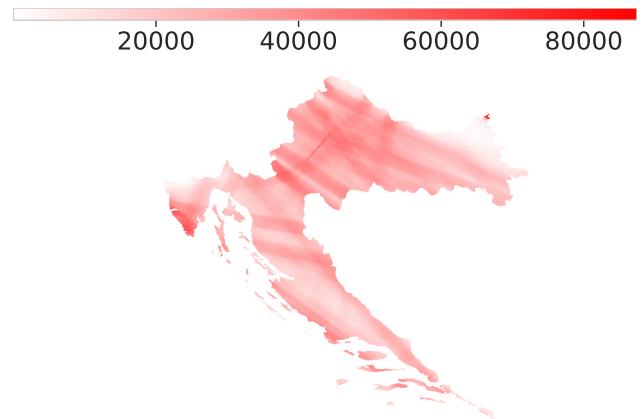


Fig. 8. Flyovers and flyovers frequency over Croatia

1) *Flight Coverage by Solar-based Imagery Types:* The daily flight coverage at different solar altitude angles is estimated to inspect how capture time impacts flight coverage.

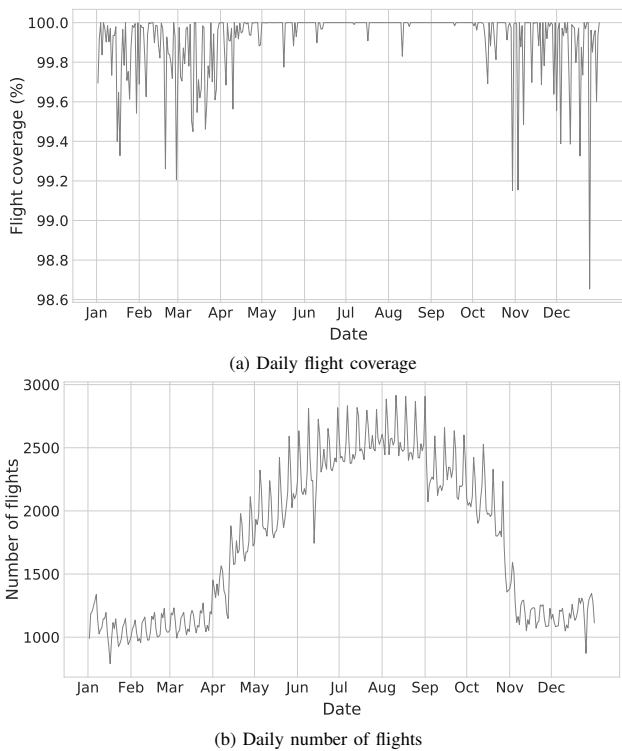


Fig. 9. Flight coverage and number of flights

The solar altitude angles (Figure 1a), represents the set of solar altitude angles rounded to the nearest integer. Figure 10a shows that the *FC* throughout the year is highest at the maximum/minimum solar altitude angle for that part of the year, known as zenith/nadir, respectively (Figure 1b). Next, we examine the duration of the solar altitude angle throughout the year (Figure 10b). We can see that the duration of the solar altitude angles is not equal. Therefore, the maximum/minimum solar altitude angle lasts longer than other solar altitude angles, giving aircraft more time to capture imagery, resulting in higher *FC*.

We also estimate flight coverage for solar-based imagery defined in Section III-A2. Figure 11 shows daily flight coverage for imagery types. On the one hand, there is a slight difference in *FC* for daytime and nighttime imagery. However, the overall *FC* is above 95% throughout the year. On the other hand, *FC* during twilight imagery ranges between 75% and 99%, which is lower than for daytime and nighttime imagery. These results are affected by different numbers of hours for each of the solar-based imagery types as shown in Figure 2. Despite significant differences in the number of hours for daytime and nighttime imagery, *FC* does not follow the same pattern. This suggests there are enough aircraft to achieve great *FC* for both, despite a 7-hour difference in some parts of the year.

Furthermore, we calculate the number of days required to achieve *FC* of 90% and 99% of the Croatian area by assuming that capturing begins on each day of the year. By using this approach it would be possible to find the best starting day to achieve desired coverage value in the shortest number of days. The number of days required to achieve *FC* of 90% is shown in Figure 12a, which is the same for daytime and

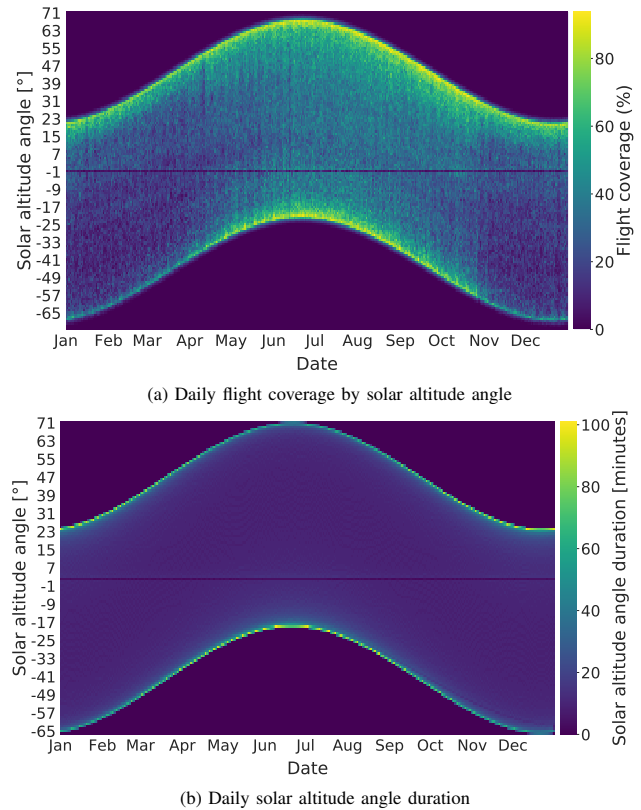


Fig. 10. Solar altitude angles and flight coverage relations

nighttime imagery. Additionally, the number of days to achieve *FC* of 99% ranges between 1 and 3 days for daytime and nighttime imagery with slight variations based on seasons. To summarize, a few days are enough to cover a good percentage of the Croatia for most parts of the year for daytime/nighttime imagery, while the highest number of days to achieve a good coverage percentage is for twilight (1-10 days).

2) *Flight Altitude Impact on Flight Coverage*: This section inspects flight altitude impact on *FC* where flight altitude value represents the set of altitude values rounded to the nearest integer. Figure 13 depicts daily total flight time per different altitudes and shows that most common altitudes are ranging from 10km to 11km, as well as up to 1km. This is because aircraft spend the majority of their time at altitudes between 0km and 1km during the landing/takeoff flight phase, and at cruising altitudes between 10km and 12km.

Additionally, *FC* is estimated for solar-based imagery types

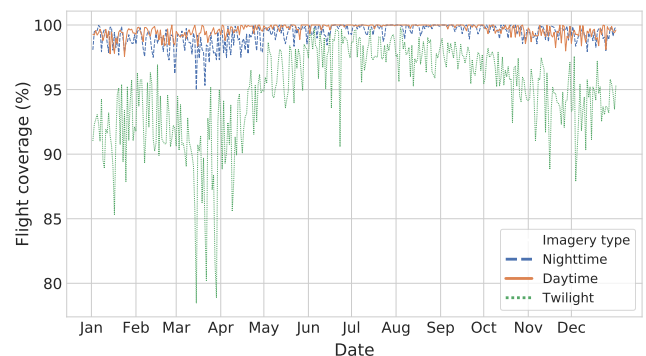
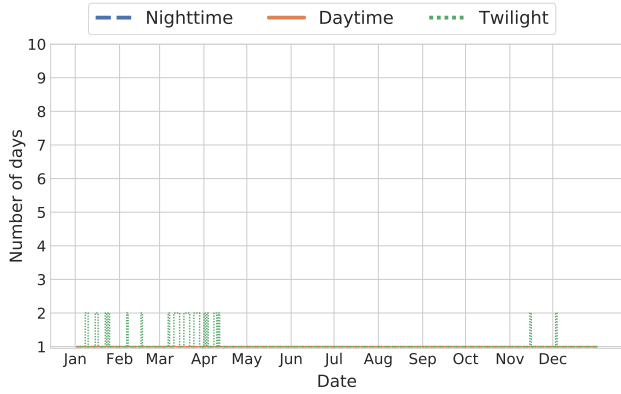
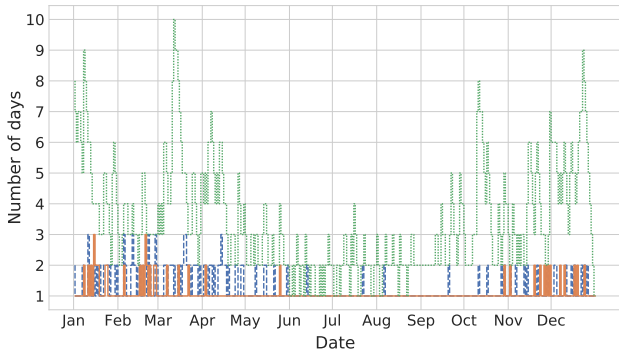


Fig. 11. Daily flight coverage solar-based imagery types



(a) Flight coverage of 90%



(b) Flight coverage of 99%

Fig. 12. Number of days to achieve flight coverage threshold

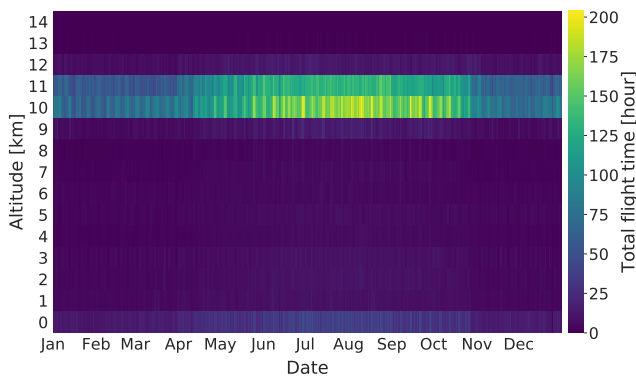


Fig. 13. Daily total flight time by flight altitudes

at different flight altitudes because altitude affects spatial resolution by making it higher at lower altitude, and lower at higher altitude. For this estimation flight altitudes are categorized using cloud categorization by altitude from Table V. Figure 14 depicts FC by solar-based imagery and flight altitudes with a significant difference between the low, medium, and high altitude flights. Firstly, FC for low altitude flights ranges from 0% to 12%, because altitude is low and field of view is reduced. Secondly, FC for altitudes between 2 and 6km ranges between 3% and 67%. Thirdly, FC for flight altitudes above 6km is between 78% and 100%. For this case values are the largest, because this is the longest period of the flight phase and the field of view is increased because altitude is highest. Furthermore, twilight imagery has the lowest FC for all three flight altitude categories due to the short duration. However, the tradeoff between altitude and field of view exists. On the one hand, taking images from higher altitudes increases the field of view, capturing a greater area with fewer details.

TABLE VII
SPATIAL RESOLUTION FOR DIFFERENT FLIGHT ALTITUDES

Flight altitude [km]	Spatial resolution [m/pixel]
1	0.129
2	0.258
6	0.775
10	1.292
14	1.809

On the other hand, if the altitude is low, the field of view is reduced, and a smaller area with more details is captured.

B. Imagery Results

The following section provides temporal and spatial resolutions of captured imagery, as well as required storage. Temporal and spatial resolutions are important aspects in the applicability of aerial imagery for various applications. As aerial imagery data can be massive, especially if captured in high resolution, the amount of required storage is examined.

1) *Temporal and Spatial Resolutions*: Temporal resolution of aerial imagery refers to the frequency at which images are captured over the same area. In our case temporal resolution is expressed as the total number of images per hour considering different overlaps. These results vary between 2,091 and 5,127 images per hour for an overlap of 0% and 60%, respectively. Additionally, we inspect what areas of Croatia are more covered with aircrafts and define temporal resolution as a number of flyovers over the base unit polygon sized $25km \times 25km$. Figure 16 depicts temporal resolution for flight altitude categories (Table V). The temporal resolution is increased for low altitude flights in airport areas, since flights only achieve lower altitudes when departing from or arriving at an airport. Next, temporal resolution for medium altitude flights is relatively uniform, because they only achieve that altitude in ascending/descending phase. In contrast to low and medium altitude flights, high altitude flights have the highest temporal resolution, since they do not have to land at Croatian airports, rather they pass over Croatia at cruising altitude.

Spatial resolution is calculated using Ground Sampling Distance, which represents the area size covered by a single pixel [14], Imperx T9040 characteristics (Table II) and various altitudes. Table VII shows that with altitude increase, spatial resolution increases linearly. Higher altitudes offer covering larger areas in a single image, with an extensive view and less details, while lower altitudes yield higher spatial resolution by distributing more pixels over the same area, with fine details.

2) *Storage Requirements*: Captured aerial imagery has to be stored. Figure 15 depicts a daily number of captured imagery as well as required storage, for overlaps 0%, 30%, and 60%, where 0% means no overlap and 60% is recommended. We can see that number of captured imagery increase during spring and summer, while it decrease during autumn and winter due to seasonal variations in flight numbers. Total storage is in the range between 5TB and 50TB and it follows the same trendline as the number of images.

The total number of imagery captured in Croatia in a year, and the amount of storage, is calculated (Table VIII). Table

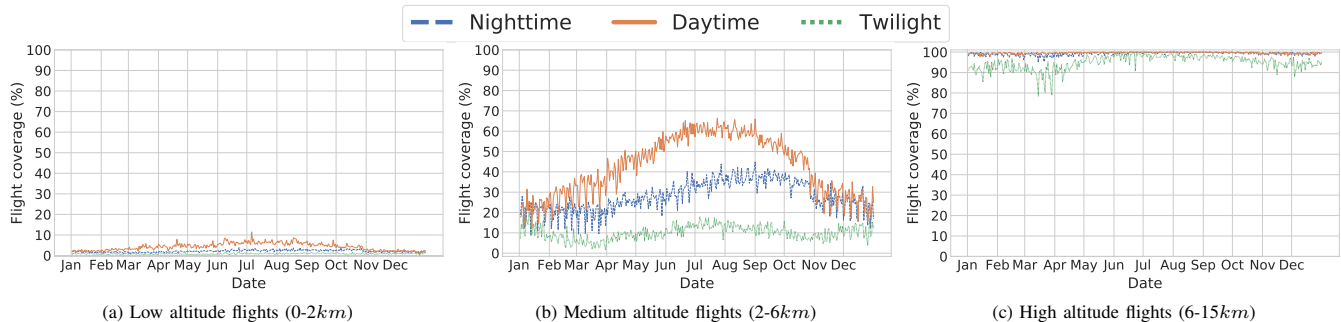


Fig. 14. Flight coverage by flight altitudes and imagery types

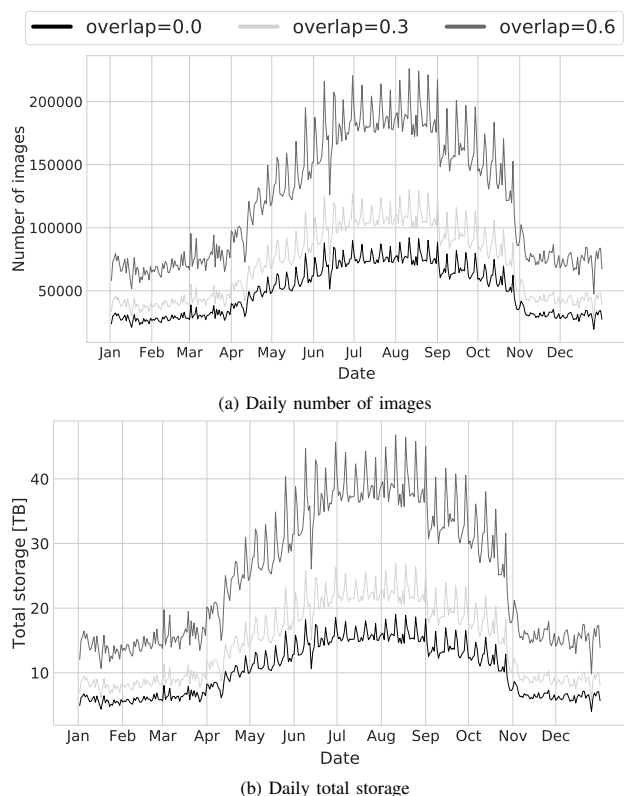


Fig. 15. Number of acquired images and storage requirements

TABLE VIII
NUMBER OF IMAGES AND REQUIRED STORAGE

Overlap (%)	Number of images	Total storage (TB)
0	18,318,842	3,792
10	20,289,717	4,200
20	22,751,369	4,710
30	25,917,730	5,364
40	30,138,362	6,238
50	36,046,542	7,461
60	44,909,261	9,926

VIII shows that even with no overlap, there is a storage requirement for 3,784 TB, while for 60% overlap it goes up to 10 PB. With the overlap increase, the number of captured images increases exponentially, resulting with the increase in the total storage, thus compromising between error tolerance and storage requirements.

C. Cloud Coverage

Cloud occurrences vary, hence Figure 18 depicts temporal monthly cloudiness over Croatia showing that high clouds are the most frequent in Croatia, while low clouds are the rarest. However, comparing all cloud types, cloud coverage is the lowest from June to September, making this period best for aerial imagery. The spatial average cloudiness for Croatia is calculated to find areas with more or fewer clouds (Figure 17). This analysis confirms that high clouds are the most present and that there is increased number of low clouds in the mountain part. Thus, we can confirm that a considerable part of Croatia can be covered with a high spatial resolution. There are slightly more medium clouds inside continental part, while high clouds are decreased in the southern part.

1) *Cloud-inclusive Flight Coverage*: In this section, we combine composite cloud coverage (CC^*) data with flight coverage (FC) data using Equations 6, 7, and 8. This analysis includes three scenarios: worst-case with maximal CC^* and minimal FC^* (FC_{min}^*, CC_{max}^*), best-case with minimal CC^* and maximal FC^* (FC_{max}^*, CC_{min}^*), and most realistic where CC^* and FC^* are random (FC_{rand}^*, CC_{rand}^*). Figure 19 depicts the difference between FC and FC^* for selected use-cases, as well as CC^* . All results are presented only for daytime imagery, for the month with the lowest and highest cloud coverage (August/November). Results from Figure 19 show that FC^* is reduced based on the CC^* . Differences between FC and FC^* are lowest for low/medium altitude flights, and highest for high altitude flights.

Flight coverage for low altitude flights is quite low (less than 10% in August, and less than 5% in November) due to short low altitude flight period. As a result, differences between FC and FC^* are minor because FC is small and clouds have a small impact on them. It is interesting to note that for the November worst-case scenario (FC_{min}^*, CC_{max}^*) is extremely close to zero. Furthermore, medium altitude flights are more represented than low altitude flights resulting in maximum FC of 65% in August, and 40% in November. Flight coverage for high altitude flights is almost 100%, however when clouds are included in calculation of FC^* worst-case for the most cloudy day for August (Aug. 14th) is around 30%, while best-case for August is almost 100% (Aug. 20th). Furthermore, FC for November can achieve 100%, however best-case (Nov. 1st) for FC^* is around 68%. Please note that low clouds include clouds up to 2km, while medium clouds (2km to 6km) and high clouds (above 6km) includes all types of clouds below.

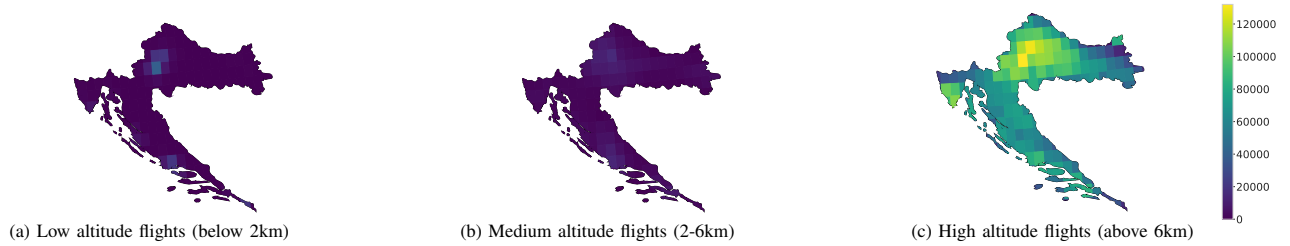


Fig. 16. Temporal resolution as number of flyovers



Fig. 17. Spatial cloud coverage - Croatia

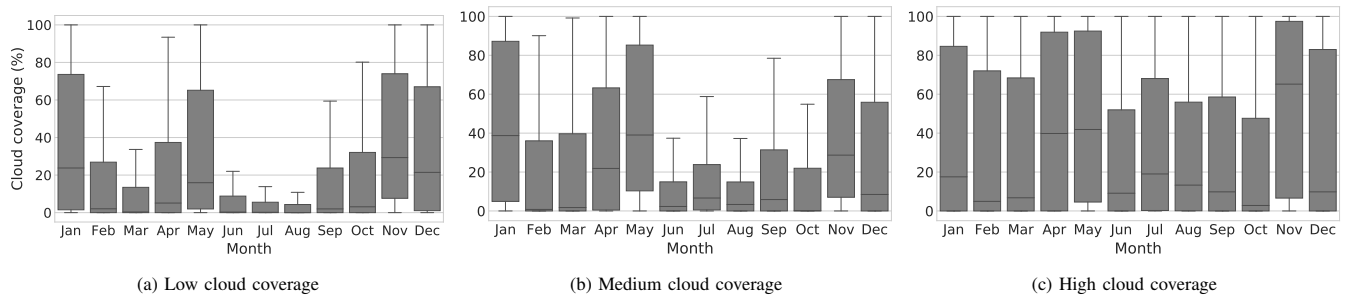


Fig. 18. Box plot visualization of cloud coverage

Minimal CC^* for November is very high and for low clouds is above 13%, while for high clouds there is no day of the November below 45%.

Figure 20 depicts FC and FC^* monthly differences. High clouds have the greatest impact on FC since they are the most common clouds, and below them may appear other clouds (Section III-C2). Low altitude flights are the rarest, hence all FC are below 40%. For medium altitude flights, FC is between 80% and 100%. However, with clouds, differences between FC and FC^* for the least cloudy month August are 33% for worst-case and 8% for best case scenario. Furthermore, for high altitude flight FC is almost 100% for every month, but with clouds less cloudy month (August) best-case FC^* is 75%, and worst-case is 38%. For November, differences between FC and best-case FC^* are 65%.

V. DISCUSSION

The cloud coverage dataset in this paper is used to adjust flight coverage by including clouds into calculation. However, the spatial resolution of this dataset is $25km \times 25km$, with a temporal resolution of one hour, and it may be adequate for this analysis. On the one hand, cloud spatial distribution can vary, and higher-resolution data should provide more exact information about the location of clouds, as well as better capture of local variations. On the other hand, clouds may change fast over time, and higher-resolution data offers more frequent updates on cloud coverage. For example, the UERA5

dataset [44] has a higher spatial ($11km \times 11km$), and temporal resolution (6 hours). In this case, we chose improved temporal resolution over spatial resolution as a compromise. Cloud coverage vary throughout the year due to factors such as weather patterns and seasonal variations in temperature and humidity [45]. Generally speaking, varies significantly across countries due to geographical and atmospheric differences [46]. Cloud coverage is generally greatest in regions with high levels of atmospheric moisture, such as tropical and equator regions [45]. For example, northern European countries have higher cloud coverage due to colder and humid climates, while southern European countries tend to have lower cloud coverage due to their warm and dry climate. Furthermore, in this paper, we defined three types of aerial imagery based on solar altitude angles, i.e. solar-based imagery. However, solar altitude angles vary by country and region due to their latitude [36]. On the one hand, countries near the equator typically have higher solar altitude angles throughout the year due to their proximity to the Sun path [36]. On the other hand, countries located at higher latitudes, endure higher seasonal variations in solar altitude angle due to their distance from the equator. During summer these countries can experience 24 hours of daylight, with the Sun remaining above the horizon for extended periods of time. However, during the winter months, these countries may experience polar nights, when the Sun remains below the horizon for extended periods of time and the solar altitude angle approaches zero. The flight dataset in this paper is used to estimate flight coverage and inspect cloud effects on it.

TABLE IX
MONTHLY DIFFERENCES BETWEEN FC AND FC^* FOR HIGH FLIGHTS

$Diff / Month$	1	2	3	4	5	6	7	8	9	10	11	12
$FC - (FC^*_{min}, CC^*_{max})$	0.93	0.69	0.68	0.82	0.95	0.57	0.67	0.62	0.75	0.7	0.98	0.86
$FC - (FC^*_{rand}, CC^*_{rand})$	0.77	0.5	0.48	0.52	0.78	0.39	0.48	0.44	0.53	0.51	0.82	0.67
$FC - (FC^*_{max}, CC^*_{min})$	0.58	0.3	0.28	0.41	0.58	0.18	0.27	0.25	0.32	0.31	0.63	0.47

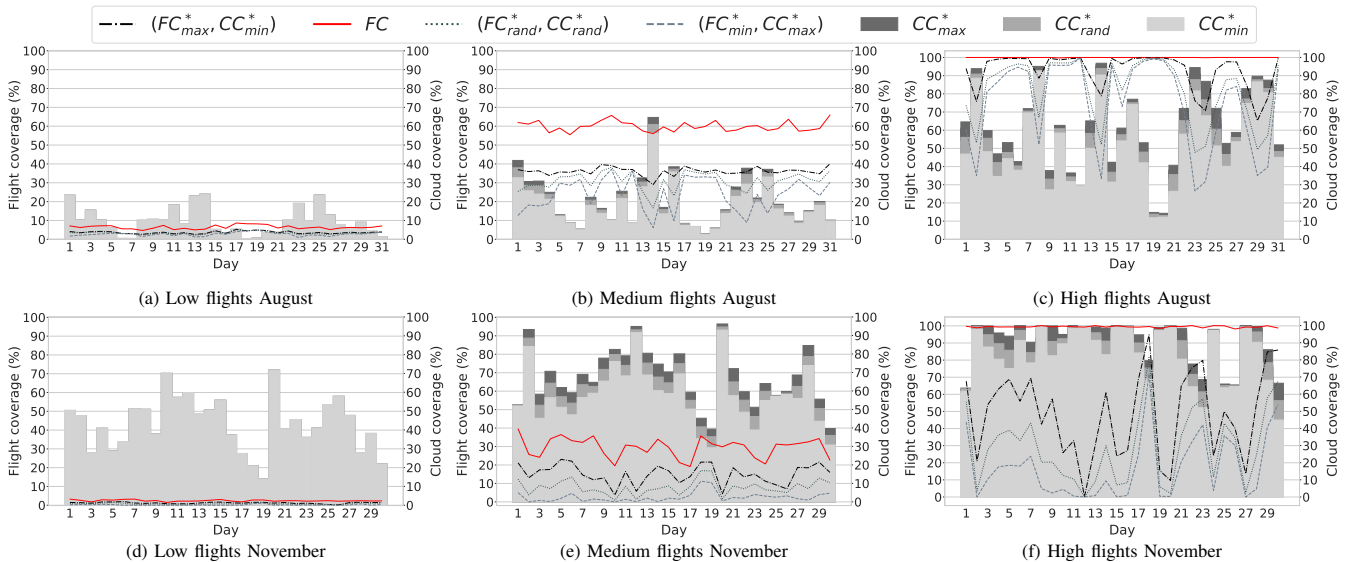


Fig. 19. Comparison of original and cloud-inclusive flight coverage for year 2019

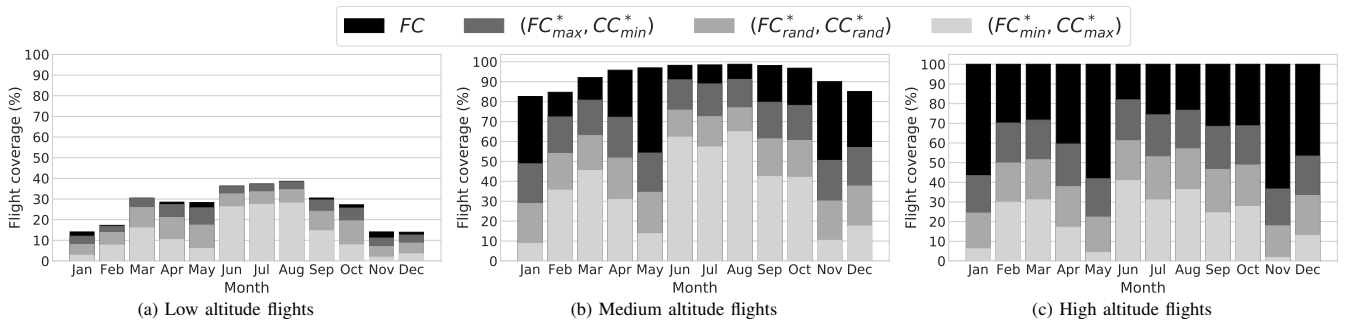


Fig. 20. Flight coverage and cloud-inclusive flight coverage comparison for different altitude flights

Clouds reduce flight coverage by affecting aerial imagery, hence we do not know if clouds overlap aerial imagery, and even if they are we can not be sure how much. Accordingly, we used three use-cases that includes the worst-case scenario where clouds totally overlap with flight polygon, best-case scenario where clouds and flight polygon have no or minimal overlap, and most realistic use-case where clouds and flights polygon overlap randomly.

VI. CONCLUSION AND FUTURE WORK

This paper presents a detailed analysis of the applicability of using commercial flights to capture aerial imagery with focus on general flight coverage of Croatia, and flight coverage at various flight altitudes and periods of the day. Furthermore, flight coverage is combined with cloud coverage to adjust flight coverage since clouds reduce the imagery usability.

The results demonstrated general daily flight coverage without clouds above 98.6%, as well as very satisfying flight

coverage without clouds above 95% for daytime and nighttime imagery, while twilight imagery offers flight coverage without clouds varying from 75% to 100%. However, when clouds are included into calculation, results are changed. Average flight coverage without clouds for low altitude flights is 26%, but worst-case cloud-inclusive flight coverage decreases to 12.5%, while best-case is 24.75%. Next, for medium altitude flights, average flight coverage without clouds is 92.52%, worst-case cloud inclusive flight coverage is 36.16% and the best-case is 72.33% in average. Furthermore, flight coverage without clouds is highest at high altitude flights because it represents the longest flight phase with largest field of view. Average flight coverage without clouds for high altitude flights is 100%, but best-case cloud-inclusive flight coverage is 61.91%, worst-case is 22.41%, and most realistic case is 42.58% which is almost 60% lower than flight coverage. The spatial and temporal resolutions are highly dependent on flight altitude, with spatial resolution ranging from 0.129 to 1.809 $m/pixels$,

while temporal resolution varies between 2,091 and 5,127 images per hour. Additionally, the storage requirements for aerial imagery are approximately 5,000 TB on average. Our study shows the feasibility of using commercial flight as a novel remote sensing system by mounting cameras on these flight. We have shown that it is possible to collect valuable Earth observation data efficiently. Furthermore, numerical results present significance within the context of Earth observation and remote sensing since it provides global coverage of Croatia and with high temporal and spatial resolution.

For future work, results could be extended to more countries and water area to explore worldwide applicability. One valuable aspect to inspect is minimum percentage of planes equipped with cameras to achieve wanted coverage threshold. Furthermore, advanced nature-inspired optimization algorithms such as Prairie Dog, Dwarf Mongoose, and Gazelle Optimization could be used to improve our flight coverage and cloud coverage models. Modified elite opposition-based artificial Hummingbird algorithms can be utilized for improving the accuracy and efficiency of our calculations.

REFERENCES

- [1] O. R. Young and M. Onoda, "Satellite earth observations in environmental problem-solving," *Satellite Earth Observations and Their Impact on Society and Policy*, p. 3–27, 2017.
- [2] Q. Zhao, L. Yu, Z. Du, D. Peng, P. Hao, Y. Zhang, and P. Gong, "An overview of the applications of earth observation satellite data: Impacts and future trends," *Remote Sensing*, vol. 14, no. 8, p. 1863, 2022.
- [3] S. H. Qader, J. Dash, V. A. Alegana, N. R. Khwarahm, A. J. Tatem, and P. M. Atkinson, "The role of earth observation in achieving sustainable agricultural production in arid and semi-arid regions of the world," *Remote Sensing*, vol. 13, no. 17, p. 3382, 2021.
- [4] M. R. Ponomarenko and V. A. Zelentsov, "Forest monitoring and analysis based on earth observation data services," *IOP Conference Series: Earth and Environmental Science*, vol. 806, no. 1, 2021.
- [5] W. Musakwa and A. van Niekerk, "Earth observation for sustainable urban planning in developing countries," *Journal of Planning Literature*, vol. 30, no. 2, p. 149–160, 2014.
- [6] S. Lang, P. Füreder, B. Riedler, and et al., "Earth observation tools and services to increase the effectiveness of humanitarian assistance," *European Journal of Remote Sensing*, vol. 53, no. sup2, p. 67–85, 2019.
- [7] J. Read and M. Torrado, "Remote sensing," *International Encyclopedia of Human Geography*, p. 335–346, 2009.
- [8] A. Matese, P. Toscano, S. Di Gennaro, L. Genesio, F. Vaccari, J. Primicerio, and et al., "Intercomparison of uav, aircraft and satellite remote sensing platforms for precision viticulture," *Remote Sensing*, vol. 7, no. 3, p. 2971–2990, 2015.
- [9] B. Bansod, R. Singh, R. Thakur, and G. Singhal, "A comparison between satellite based and drone based remote sensing technology to achieve sustainable development," *Journal of Agriculture and Environment for International Development*, vol. 111, no. 01, pp. 383–407, 2017.
- [10] P. Dorji and P. Fearn, "Impact of the spatial resolution of satellite remote sensing sensors in the quantification of total suspended sediment concentration: A case study in turbid waters of northern western australia," *PLOS ONE*, vol. 12, no. 4, 2017.
- [11] X. Luo, M. Wang, G. Dai, and X. Chen, "A novel technique to compute the revisit time of satellites and its application in remote sensing satellite optimization design," *International Journal of Aerospace Engineering*, vol. 2017, p. 1–9, 2017.
- [12] Z. Kavooosi, M. H. Raoufat, M. Dehghani, J. Abdolabbas, S. A. Kazemini, and M. J. Nazemossadat, "Feasibility of satellite and drone images for monitoring soil residue cover," *Journal of the Saudi Society of Agricultural Sciences*, vol. 19, no. 1, p. 56–64, 2020.
- [13] Y. Li, W. Yan, S. An, W. Gao, J. Jia, S. Tao, and W. Wang, "A spatio-temporal fusion framework of uav and satellite imagery for winter wheat growth monitoring," *Drones*, vol. 7, no. 1, p. 23, 2022.
- [14] T. Mastelic, J. Lorincz, I. Ivandic, and M. Boban, "Aerial imagery based on commercial flights as remote sensing platform," *Sensors*, vol. 20, no. 6, p. 1658, 2020.
- [15] "Skyflox." <https://skyflox.eu>. Accessed: 24-05-2023.
- [16] P. Kansakar and F. Hossain, "A review of applications of satellite earth observation data for global societal benefit and stewardship of planet earth," *Space Policy*, vol. 36, p. 46–54, 2016.
- [17] DIITET, "Technologies for aerospace and earth observation - whitepaper," *DIITET*, p. 9, 2018.
- [18] H. Jafarbiglu and A. Pourreza, "A comprehensive review of remote sensing platforms, sensors, and applications in nut crops," *Computers and Electronics in Agriculture*, vol. 197, p. 106844, 2022.
- [19] "Unoosa, united nations office for outer space affairs." <https://www.unoosa.org>. Accessed: 24-05-2023.
- [20] "Nasa, the national aeronautics and space administration." <https://www.nasa.gov>. Accessed: 24-05-2023.
- [21] G. Survey, "Landsat earth observation satellites," *Fact Sheet*, p. 4, 2015.
- [22] F. Prata and M. Lynch, "Passive earth observations of volcanic clouds in the atmosphere," *Atmosphere*, vol. 10, no. 4, p. 199, 2019.
- [23] A. Krimchansky, D. Machi, S. A. Cauffman, and M. A. Davis, "Next-generation geostationary operational environmental satellite (goes-r series): A space segment overview," *SPIE Proceedings*, 2004.
- [24] Airbus, "Airbus oneatlas - whitepaper," *Airbus*, 2021.
- [25] C. Cohen, "Early history of remote sensing," *Proceedings 29th Applied Imagery Pattern Recognition Workshop*, p. 3, 2000.
- [26] E. T. Young, E. E. Becklin, and P. M. Marcum, "Early science with sofia, the stratospheric observatory for infrared astronomy," *The Astrophysical Journal*, vol. 749, no. 2, 2012.
- [27] NASA, "Er-2 high-altitude airborne science aircraft," *NASA, Fact Sheet*, p. 2, 2015.
- [28] "Cessna 206." <https://impact.earthdata.nasa.gov/casei/platform/Cessna%20206>. Publisher: NASA, Accessed: 24-05-2023.
- [29] H. Yao, R. Qin, and X. Chen, "Unmanned aerial vehicle for remote sensing applications—a review," *Remote Sensing*, vol. 11, no. 12, p. 1443, 2019.
- [30] M. Sabour, P. Jafary, and S. Nematian, "Applications and classifications of unmanned aerial vehicles: A literature review with focus on multi-rotors," *The Aeronautical Journal*, vol. 127, no. 1309, p. 466–490, 2023.
- [31] "Aircraft manufacturing company." <https://www.jouav.com/blog/drone-with-longest-flight-time.html>. Publisher: JOUAV, Accessed: 24-05-2023.
- [32] Wingtra, "Down to 1 cm (0.4 in) in drone survey accuracy - whitepaper," *Wingtra*, 2018.
- [33] "Airbus." <https://www.airbus.com>. Accessed: 24-05-2023.
- [34] H. Zhang, B. Li, J. Zhang, and F. Xu, "Aerial image series quality assessment," *IOP Conference Series: Earth and Environmental Science*, vol. 17, p. 012183, 2014.
- [35] P. M. Dare, "Shadow analysis in high-resolution satellite imagery of urban areas," *Photogrammetric Engineering and Remote Sensing*, vol. 71, no. 2, p. 169–177, 2005.
- [36] S. Kalogirou, "Solar thermal systems," *Comprehensive Renewable Energy*, p. 1–25, 2012.
- [37] J. Kovalevsky and K. Seidelmann, "Astronomical phenomena," *Fundamentals of Astrometry*, p. 307–322, 2004.
- [38] D. Herdiwijaya, "On the beginning of the morning twilight based on sky brightness measurements," *Journal of Physics: Conference Series*, vol. 1523, no. 1, p. 012007, 2020.
- [39] "Flightradar24 dataset." <https://www.flightradar24.com/>. Accessed: 06-03-2023.
- [40] D. Paine and J. Kiser, *Aerial Photography Image Interpretation: Third Edition*. Wiley, 02 2012.
- [41] H. Hersbach, B. Bell, P. Berrisford, G. Biavati, A. Horányi, J. Muñoz Sabater, J. Nicolas, C. Peubey, R. Radu, I. Rozum, D. Schepers, A. Simmons, C. Soci, D. Dee, and J.-N. Thépaut, "Era5 hourly data on single levels from 1959 to present." Accessed: 06-03-2023.
- [42] R. J. Hogan and A. J. Illingworth, "Deriving cloud overlap statistics from radar," *Quarterly Journal of the Royal Meteorological Society*, vol. 126, no. 569, p. 2903–2909, 2000.
- [43] A. M. Tompkins and F. Di Giuseppe, "An interpretation of cloud overlap statistics," *Journal of the Atmospheric Sciences*, vol. 72, no. 8, p. 2877–2889, 2015.
- [44] "Uerra regional reanalysis for europe on single levels from 1961 to 2019." Accessed: 21-03-2023.
- [45] "Cloudy earth." <https://earthobservatory.nasa.gov/images/85843/cloudy-earth>. Publisher: NASA, Accessed: 04-04-2023.
- [46] "Countries by cloud cover." <https://www.extremeweatherwatch.com/countries-by-cloud-cover>. Accessed: 04-04-2023.



Dinko Zidic received a bachelor's degree and master's degree in computer science from the Faculty of Electrical Engineering, Mechanical Engineering, and Naval Architecture, University of Split, Croatia in 2019 and 2021. During the last two years of his study, he worked as a student helper at Research Department in Ericsson Nikola Tesla, Split and gain knowledge about spatio temporal data analytics and storage solutions, cloud microservice architecture, along with the concept of Digital Twin. Today, he works as a Researcher at Ericsson Nikola Tesla.



Jelena Culic Gambiroza is currently employed as a Researcher at Ericsson Nikola Tesla, Split, Croatia. She received her bachelor and master's degree in Computer Science from Faculty of Electrical Engineering, Mechanical Engineering and Naval Architecture, University of Split, Croatia, in 2013 and 2015, respectively. She is currently pursuing the PhD degree at the University of Split. Her research interests include Big Data challenges in Internet of Things (IoT) as well as Data analytics including Statistical Methods and Machine Learning.



Toni Mastelic is a researcher at Ericsson Nikola Tesla d.d., Research department. He did his bachelor and masters studies in Computer Science at the University of Split, FESB, Croatia, where he received his Bachelor degree in 2009, and Master degree in 2011. Afterwards, he worked as a research and later on as university assistant at Vienna University of Technology, where he pursued his PhD. Finally, he received his PhD degree in 2015 at the Institute of Software Technology and Interactive Systems, Vienna University of Technology.



Mario Cagalj received the Dipl.Ing. degree in computer science and electrical engineering from the University of Split, Croatia, in 1998, and the Ph.D. degree in communication systems from the École Polytechnique Fédérale de Lausanne (EPFL), Lausanne, Switzerland, in 2006. He is currently employed as a Full Professor with the Faculty of Electrical Engineering, Mechanical Engineering and Naval Architecture (FESB), University of Split. His research interests encompass security protocols for wireless networks, applied cryptography, game theory in networks, and energy-efficient communication protocols for wireless networks.

theory in networks, and energy-efficient communication protocols for wireless networks.